Article

Pcdh19 mediates olfactory sensory neuron coalescence during postnatal stages and regeneration

MOR28 OSNs are divided into two clusters

Pcdh19 mutant

Differential effect on lateral glomeruli

Andrew P.
Martinez,
Alexander C.
Chung, Suihong
Huang, ..., Jin Y.
Kim, Jean Y.H.
Yang, David M. Lin

DML45@cornell.edu

Highlights

A mutation in *Pcdh19* affects coalescence of MOR28 OSNs during regeneration

Lateral coalescence is more strongly affected than medial

Males are more strongly affected than females

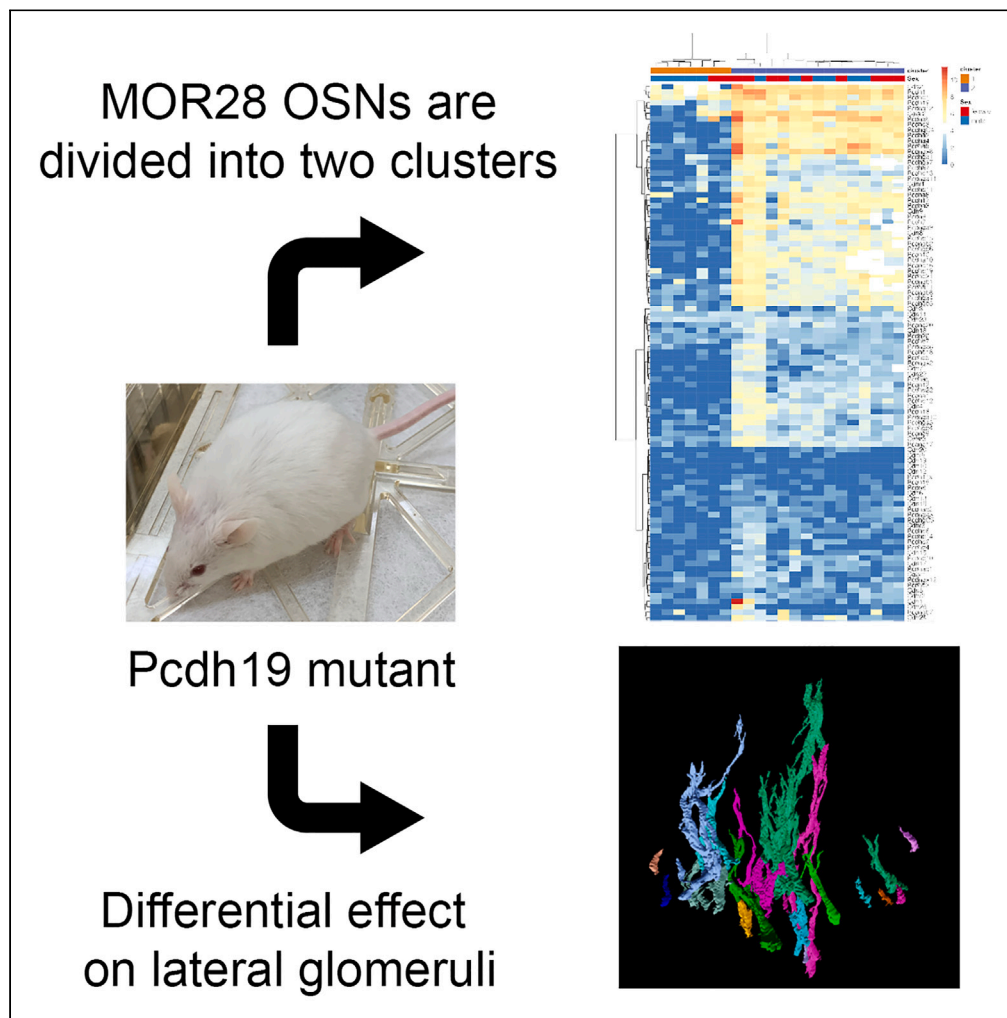MOR28 OSNs can be subdivided into two large clusters based on gene expression

Article

Pcdh19 mediates olfactory sensory neuron coalescence during postnatal stages and regeneration

Andrew P. Martinez,[1] Alexander C. Chung,[1] Suihong Huang,[2] Adam J. Bisogni,[1] Yingxin Lin,[3] Yue Cao,[3] Eric O. Williams,[1] Jin Y. Kim,[4] Jean Y.H. Yang,[3] and David M. Lin[1,5,*]

SUMMARY

The mouse olfactory system regenerates constantly throughout life. While genes critical for the initial projection of olfactory sensory neurons (OSNs) to the olfactory bulb have been identified, what genes are important for maintaining the olfactory map during regeneration are still unknown. Here we show a mutation in *Protocadherin 19* (*Pcdh19*), a cell adhesion molecule and member of the cadherin superfamily, leads to defects in OSN coalescence during regeneration. Surprisingly, lateral glomeruli were more affected and males in particular showed a more severe phenotype. Single cell analysis unexpectedly showed OSNs expressing the MOR28 odorant receptor could be subdivided into two major clusters. We showed that at least one protocadherin is differentially expressed between OSNs coalescing on the medial and lateral glomeruli. Moreover, females expressed a slightly different complement of genes from males. These features may explain the differential effects of mutating *Pcdh19* on medial and lateral glomeruli in males and females.

INTRODUCTION

A remarkable feature of the vertebrate olfactory system is its ability to regenerate throughout life.[1,2] During development, each olfactory sensory neuron (OSN) will extend an axon from the nasal epithelium into the olfactory bulb. OSNs expressing a common odorant receptor will coalesce to form medial and lateral glomeruli situated at relatively stereotyped locations within the bulb.[3–5] The remarkable fidelity with which this olfactory map is formed in rodents has led to intensive efforts to identify genes responsible for this process.[6,7]

The guidance mechanisms involved during early development, however, appear to differ from those used during later postnatal stages and in regeneration. Genetic analyses identified a critical period needed to establish the initial olfactory map in rodents.[8–10] Neurons born prior to the ~first week of postnatal life are essential for establishing the map. In the absence of these early, "navigator" neurons, later born neurons failed to coalesce.

These studies raise the question as to what mechanisms guide later born OSNs during regeneration. In one model, later born OSNs use adhesion molecules to follow navigator neuron axons to their appropriate glomerular location.[8–10] To date however, what function adhesion molecules play in regeneration has not been tested. Furthermore, how adhesion molecules might influence medial and lateral projection patterns during regeneration is also unknown.

To begin addressing these questions, we have examined the role of *Protocadherin 19* (*Pcdh19*), a cell adhesion molecule, for its function in OSN coalescence during postnatal stages and during regeneration. *Pcdh19* is one of nine members of the delta protocadherin family which in turn is part of the cadherin superfamily.[11,12] Delta protocadherins have been previously implicated in OSN function. We showed individual OSNs express between zero and seven family members,[13] indicating broad expression among OSNs during early postnatal life. Moreover, delta protocadherin protein is detectable within axons and in glomeruli during development and in the adult.[14,15] We also demonstrated mis- and over-expression of delta *Pcdh10* led to a transient effect on the glomerular position of OSNs expressing the SR1 odorant receptor.[16] More recently, optogenetic stimulation demonstrated *Pcdh10* expression is regulated downstream of the odorant receptor itself.[17]

Among the delta family members, *Pcdh19* has been identified as the causative mutation behind a form of epilepsy known as *Pcdh19*-related epilepsy.[18] More than 270 mutations have been identified,[19] leading it to be called the second most important gene in epilepsy.[20] *Pcdh19*-related epilepsy follows an unusual inheritance pattern. *Pcdh19* is located on the X chromosome, but mutations in *Pcdh19* predominantly affect heterozygous females and not hemizygous males. Because females are mosaic, the cellular interference model proposes that

[1]Department of Biomedical Sciences, Cornell University, Ithaca, NY 14850, USA
[2]Jockey Club College of Veterinary Medicine and Life Sciences, City University of Hong Kong, Hong Kong SAR, China
[3]School of Mathematics and Statistics, F07 University of Sydney, NSW 2006, Australia
[4]Department of Biomedical Sciences, City University of Hong Kong, Hong Kong SAR, China
[5]Lead contact
*Correspondence: DML45@cornell.edu
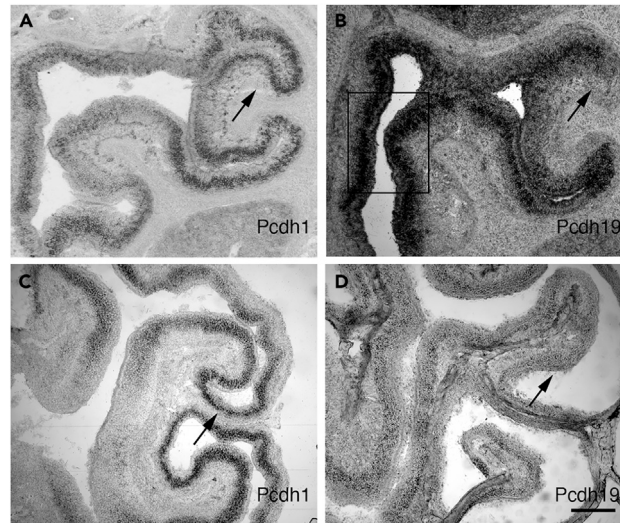https://doi.org/10.1016/j.isci.2023.108220

Figure 1. Delta protocadherin expression in the epithelium

(A–D) *Pcdh19* and *Pcdh1* were assessed for expression at E17 (A and B) and in adulthood (C and D). (A) *Pcdh1* is spatially differentially expressed in E17 epithelia, with notable enrichment in certain regions of the epithelium (e.g., black arrow).

(B) *Pcdh19* is expressed in a distinctly different pattern from *Pcdh1*, with weaker expression dorsolaterally (black arrow; compare (A) and (B)), and stronger expression medially (boxed region).

(C and D) Adult epithelial expression of *Pcdh1* (C) and *Pcdh19* (D). Only a portion of the dorsolateral epithelium is shown (black arrows), corresponding to the analogous region indicated with black arrows in (A) and (B). Scale bar:25 μm.

cells expressing the mutant copy of *Pcdh19* "interfere" with those expressing the normal form, potentially due to altered patterns of cell adhesion. This model has now been supported by *in vitro* adhesion assays, where cells expressing a mutated copy of *Pcdh19* will not adhere to cells expressing the normal protein.[21] Further, in a mutant mouse model of *Pcdh19*, cells within the brain that express the normal form of *Pcdh19* clearly segregated from those that express the mutant form.[21] Thus, mutations in *Pcdh19* are thought to affect cell-cell adhesion, migration and cell sorting.[22,23]

We generated a mutant mouse that recapitulates a known nonsense mutation of *Pcdh19* found in humans. We compared the impact of this mutation on OSN coalescence during postnatal stages and regeneration. During postnatal stages, we identified an increase in the number of glomeruli formed, consistent with a role for *Pcdh19* in the terminal stages of coalescence. During regeneration, gross defects in coalescence were seen among OSNs expressing the MOR28 odorant receptor. Interestingly, these effects differ in severity between medial and lateral glomeruli and between male and female mice at both stages. Single cell analysis showed OSNs could be subdivided into two large clusters distinguished by the expression of delta protocadherins and other cadherin superfamily members. This analysis also indicated differences in expression between males and females. We confirmed at least one delta family member appears to be differentially expressed between MOR28 medial and lateral glomeruli, potentially providing an explanation for the differential impact of mutating *Pcdh19* on OSN coalescence.

RESULTS

Pcdh19 expression is grossly maintained within the epithelium

To ask if *Pcdh19* is present during different stages of OSN coalescence, we examined its expression pattern at different time points. As we previously showed for other delta family members,[13] at embryonic day 17 (E17), *Pcdh19* was expressed in a punctate pattern within the sensory neuron layer (Figure 1B). Interestingly, this expression pattern was not always uniform, but instead could be enriched in specific regions. For example, *Pcdh19* was expressed more strongly in the medial epithelium (Figure 1B, boxed area) and more weakly in the dorsolateral region (black arrow). This pattern of expression was grossly maintained through adulthood (compare Figure 1B [E17] vs. 1D [adulthood]). With the exception of *Pcdh10* (whose expression we previously showed is modified by odorant-evoked activity as the animal ages[16]), other members (*Pcdh1*, compare Figure 1A [E17] vs. 1C [adulthood]) were also maintained in grossly similar patterns throughout adulthood.

Generation of *Pcdh19^E48X^* mutant mice

To ask how *Pcdh19* influences OSN coalescence, we used CRISPR to generate a mouse mutant that recreates a known nonsense mutation (*Pcdh19^E48X^*) identified in humans[24] (Figure S1A). This mutation was originally identified as a heritable familial mutation, and affected daughters that inherit the mutation show similar timing and onset of seizure activity. This particular mutation is at the N-terminus of the protein (~25 amino acids downstream of the signal peptide). Because off-target effects of CRISPR generated animals is a potential concern, we first outcrossed mice six generations to FVB animals to reduce the likelihood of retaining an off-target mutation. Subsequent crosses to marker strains (see following text) further reduce the likelihood of off-target effects confounding our interpretation of the results.

This mutant differs from previously generated *Pcdh19* mouse mutants which delete or modify the extracellular domain.[23,25–27] We took three complementary approaches to examine our mutant for its impact on *Pcdh19* expression and function. First, we expect that the introduction of this mutation will lead to nonsense mediated decay of the mRNA. We found using qRT-PCR that our mice displayed reduced transcription of *Pcdh19* mRNA, consistent with nonsense mediated decay (Figure S1B). Although we presumed that the protein was no longer expressed due to the presence of the nonsense mutation, ~50% of the mRNA still remained (Figure S1B). It was formally possible that cryptic start sites downstream of the mutation might somehow still mediate adhesion. We therefore used the well-established K562 cell adhesion assay[13] to assess the impact of this remaining mRNA on K562 adhesion. We transfected K562 cells with a *Pcdh19*[E48X]-GFP construct. No adhesion was observed (Figure S1D), similar to cells transfected with a control N1-GFP construct (Figure S1C). Even if cryptic methionines were somehow still active, the amino acids in the first extracellular domain upstream of these putative start sites are essential for *Pcdh19* adhesion based on the crystal structure.[28,29] We confirmed this by expressing a construct that deletes the first extracellular domain (*Pcdh19*[Δ1]-GFP), which was unable to promote adhesion (Figure S1E). To show that these cells were still capable of adhesion, we co-transfected cells with *Pcdh19*[E48X]-GFP and a construct expressing the extracellular and transmembrane domains of *Pcdh19* fused to RFP (*Pcdh19*ECTM-RFP). We previously showed this construct is capable of promoting K562 cell adhesion.[13] As expected, these cells formed aggregates (Figures S1F–S1H). This co-expression experiment also shows that any truncated products produced by the mutant construct, if they exist, are not capable of interfering with normal *Pcdh19* adhesive function.

Finally, although we were unable to identify an antibody that could detect PCDH19 protein in western blots, we successfully found one that could be used for immunohistochemistry. We performed immunohistochemistry on control and *Pcdh19*[E48X] mutant mice. PCDH19 could readily be seen in control samples while no detectable protein was seen in mutants (Figures S1I and S1J). Collectively, these results show that the *Pcdh19*[E48X] mutation leads to nonsense mediated decay, is unlikely to produce any truncation products capable of mediating adhesion and leads to no detectable protein *in vivo* using immunohistochemistry.

Pcdh19[E48X] mutants display an increased number of glomeruli on the lateral surface during postnatal stages

We first asked whether or not the *Pcdh19*[E48X] mutant affected OSN coalescence during postnatal stages. We crossed the mutant mouse with the MOR28-GFP marker strain, which labels OSNs expressing the MOR28 odorant receptor. MOR28 OSNs will project to either the medial or lateral aspect of the bulb and coalesce with other MOR28 expressing OSNs to form glomeruli. We examined mice for an impact on MOR28 OSN coalescence at postnatal day 13 (P13), 20–22 (P20–P22), and at 6 weeks. We then counted how many glomeruli were present at the medial or lateral surface ("half-bulb") of each bulb. We separately assessed male controls, hemizygous males, heterozygous females, and homozygous female littermates.

Unexpectedly, we found an unusual distribution of effects that were location, age, and sex dependent. First, we found that only lateral glomeruli were significantly affected in *Pcdh19*[E48X] mice. In P13 control animals, we observed only one lateral glomerulus most of the time (92%; 1.07 glomeruli/half-bulb, Figures 2A and 2E). On rare occasions, controls displayed two lateral projections (Figures 2C and 2E) but the second projection was noticeably smaller than the primary projection. In contrast, we observed 53% of mutant male mice possessed two or sometimes three lateral glomeruli (average of 1.53 glomeruli/half-bulb), and often these were of roughly equal size (Figures 2D and 2E). Female mutants had a somewhat lesser effect (Figures 2B and 2E, 33% with more than one glomerulus, average of 1.35 glomeruli/half bulb). Although the effect did not reach significance, the phenotype seen in heterozygotes mirrors that seen in mutant mice (Figure 2E). No statistically significant effect was observed along the medial surface at P13 (Figure 2F).

We observed this phenotype appeared to have a sex dependent effect. Although both male and female mice had increased numbers of lateral glomeruli relative to male controls, male mice were more strongly affected (Figure 2E).

We then asked whether or not these effects resolved or persisted at later stages. At P20–P22, approximately one week after our initial observations, we found no significant differences in glomerular number among any genotype, sex, or glomerular location (Figures S2A and S2B). Similarly, an examination of six-week-old mutant mice showed no significant differences relative to control (Figures S2C and S2D).

Pcdh19[E48X] mice have defects in coalescence during regeneration

We next examined whether *Pcdh19* plays a role during regeneration to compare the effects (if any) against those seen during postnatal stages. We treated two to three-month-old mutant and control littermates with methimazole, a drug that induces widespread ablation of OSNs and subsequent regeneration.[30] We optimized the amount of methimazole to ensure consistent ablation of the epithelium in our mice (Figure S3). Although we cannot guarantee complete ablation, this treatment severely disrupted epithelial structure and coalescence. We performed a pilot study to assess the rate of regeneration after two, three, and four weeks after treatment, and glomeruli were clearly visible within the bulb at four weeks. We therefore examined regeneration of MOR28-GFP positive OSNs at four weeks post ablation. We again distinguished animals by sex and genotype, and separately assessed medial and lateral glomeruli. In control male animals, we observed a higher number of glomeruli at both surfaces. This is consistent with prior studies which demonstrated increased errors and glomerular formation following chemical ablation.[31,32] Similarly, we also saw more stray projections which had not coalesced with the main glomerulus. In mutant animals, however, this phenotype was greatly exacerbated. We saw greater numbers of glomeruli of varying size, as well as a broad profusion of projections. We were unable, however, to clearly resolve the patterns with standard epifluorescence.

We therefore utilized CUBIC (clear, unobstructed brain/body imaging cocktails and computational analysis) protocols to clear the tissue and preserve GFP fluorescence[33] followed by light sheet microscopy. We saw clear differences in coalescence between mutants and heterozygous females as compared to controls (Figures 3A–3H). We assessed the phenotype using three successively more circumscribed metrics. In
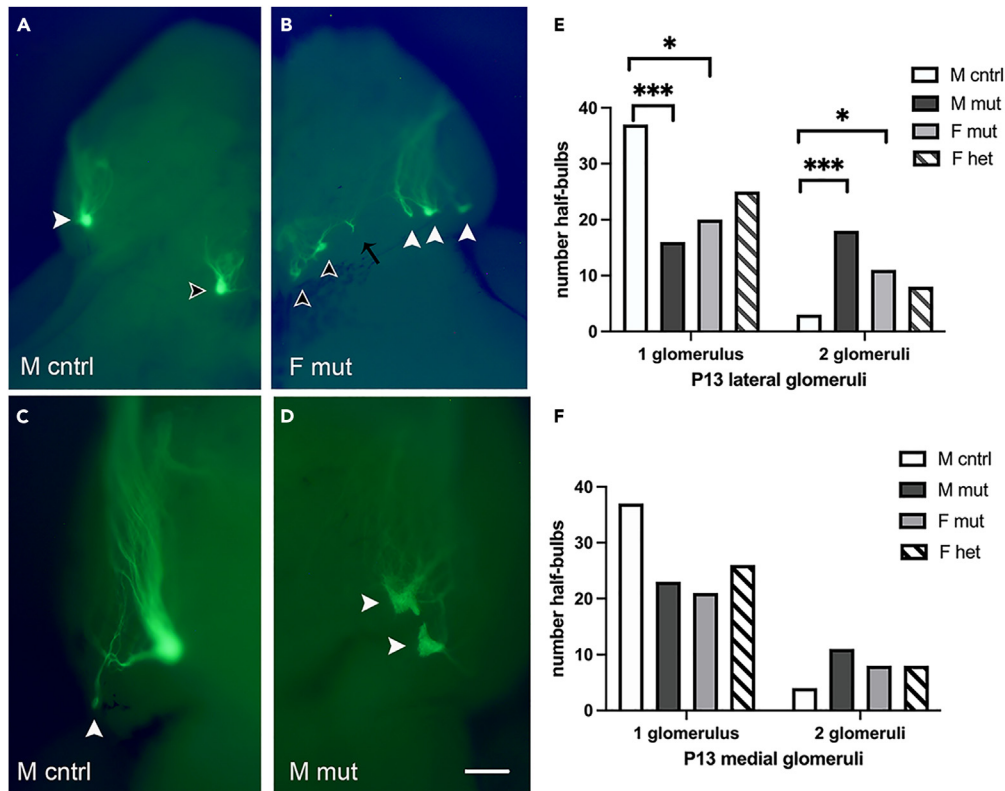
Figure 2. *Pcdh19^{E48X}* mice possess increased numbers of lateral glomeruli at P13

(A) Control mice display the canonical single medial (black arrowhead) and lateral (white arrowhead) glomerulus within the bulb.

(B) In mutants, there were more frequent examples of lateral glomeruli with two or rarely three (white arrowheads) lateral projections. We also found examples of medial glomeruli with multiple projections (black arrowheads). On occasion, examples of stray projections (black arrow) were also seen, although these smaller projections were not counted as additional glomeruli.

(C) Male control mice almost exclusively (92%) had a single glomerulus at the lateral position, with an occasional secondary projection much smaller than the primary projection (white arrowhead).

(D) Male mutant with two glomeruli on the lateral surface of approximately equal size (white arrowheads).

(E) Lateral glomeruli were increased in number for both male and female mutants.

(F) Medial glomeruli numbers were not significantly different from control. Fisher's exact test with Bonferroni correction. Scale bar: 500 μm (A and B) or 200 μm (C and D). $*p < 0.05$, $***p < 0.005$. n=22 (M cntrl), 19 (M mut), 18 (F mut). and 19 (F het).

the first, we determined the overall volume of the projection pattern. During development, OSN populations are thought to first project to their approximate glomerular region within the bulb, and then coalesce within this region to form glomeruli.[34,35] We therefore asked if the volume of this region is altered in our mutant. In the second, we assessed the number of projections present within this volume. And in the third, we quantified the proportion of OSNs present within each projection based on the distribution of GFP signal.

We performed two calculations to first assess the volume of the projection region. We calculated the size of a three-dimensional bounding box needed to encompass the spread of projections within each animal. We found no differences between mutant, heterozygous, and control mice in terms of the space taken up by the projections (Figures S4A and S4C). Next, we measured the average distance from each projection to the largest projection (based on GFP intensity). This would provide an alternative approach to assess the spread of signals surrounding the primary projection. We again found no obvious differences using this metric (Figures S4B and S4D), supporting the conclusion that the overall size of the initial projection pattern is unchanged in mutant animals.

Second, we asked whether or not the number of projections within the region had changed. For this analysis, we counted the number of projections that comprised 3% or more of overall GFP expression within each image stack (Figure 3I). We chose 3% as a floor because weakly expressing projections were difficult to consistently detect and assess. OSNs from control mice coalesced to form approximately 1.6 projections on average on the lateral surface. In contrast, mutant mice projected to multiple targets. Mutant males had the most projections (x = 6.5) as compared to female mutants (x = 5.2) and female heterozygotes (x = 6), but all genotypes and sexes were significantly different in projection number from control males (Figure 3I).

Third, we examined the distribution of GFP within the various projections. The projection bearing the largest percentage of GFP was called the primary projection. In control mice, the majority of OSNs projected to a common glomerular location, with a few stray projections. Thus,
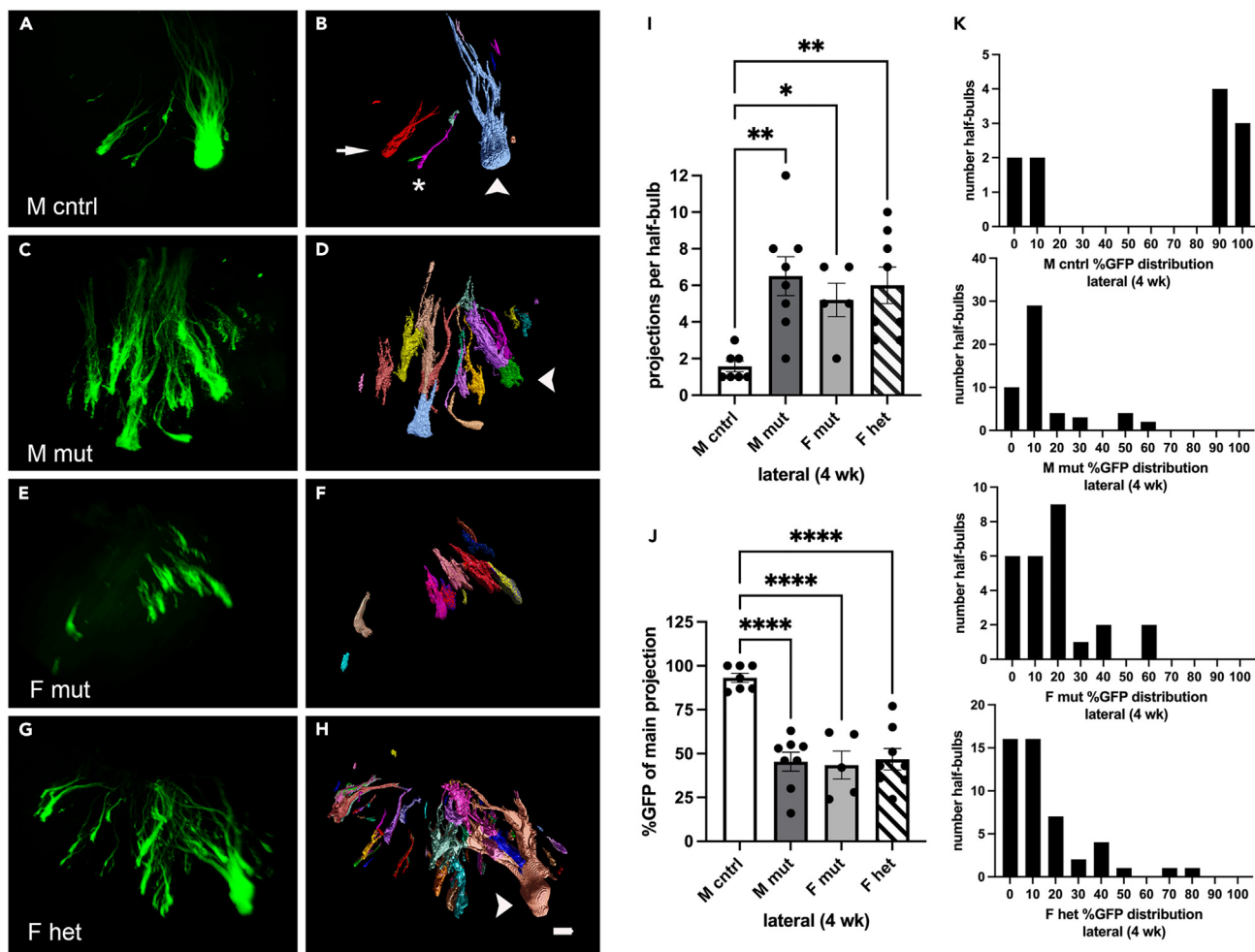
Figure 3. The *Pcdh19^(E48X)* mutation affects MOR28 OSN lateral coalescence during regeneration

(A–H) Projection of image stack obtained by light sheet microscopy (A, C, E, and G) and segmented to define projection patterns on the lateral surface (B, D, F, and H). (B, D, and H) Arrowhead indicate primary glomerular projection based on percent GFP expression relative to other projections (e.g., arrow in (B)). Asterisk in (B) indicates a projection that comprises less than 3% of the total GFP signal in the image stack. No primary projection could be easily determined in some samples (F).

(I) The number of lateral projections per half-bulb is increased in mutant and heterozygous animals.

(J) The percent of total GFP present in the main projection is significantly different between control and mutant and heterozygous mice.

(K) Histogram of distribution of GFP expression within each projection (greater than 3%) in the various genotypes. Scale bar: 100 μm. One-way ANOVA (I) $F_{(3,21)}$ = 6.16 (J) $F_{(3,21)}$ = 18.25, Dunnett's test. *p < 0.05, **p < 0.01; ****p < 0.0001. n = 7 (M cntrl), 8 (M mut), 5 (F mut), and 8 (F het).

---

on average 93% of all observed GFP was present in the main projection in control mice. In contrast, in male and female mutants, as well in heterozygous females, the proportion of GFP signal was distributed among more targets. On average, the primary projection in these mice possessed 43–47% of total GFP expression (Figure 3J). In some cases (e.g., Figure 3F), there was no obvious "primary" projection.

The strikingly varied distribution of GFP expression between control animals and mutants is particularly evident in the histograms (Figure 3K). In control mice, GFP signal was distributed at the extreme ends of the scale. That is, projections either contained 90%+ or 3–10% of the total GFP present, indicating most of the OSNs are contained within the primary projection. In contrast, in male mutants, most of the signal was on the far left of the spectrum, indicating most projections possessed between 10 and ~50% of total GFP signal. This underscores the breadth and profusion of projections. Similar patterns were observed for female mutants and heterozygotes.

We also found that, unlike during postnatal stages, medial glomeruli were affected (Figure 4). We performed the same analysis as described for the lateral glomerulus in Figure 3. All genotypes and sexes were affected. Interestingly, the degree of difference between mutants and controls on the medial surface was less than that seen for the lateral surface (Figure 3), similar to what was observed at P13 (Figure 2). Males were more affected by the *Pcdh19^(E48X)* mutation, both in the number of projections (Figure 4I) and in the distribution of GFP (Figures 4J and 4K).

During postnatal stages, the phenotype observed in lateral glomerular number at P13 was corrected by P20–P22. We therefore asked whether or not the phenotype observed at four weeks post methimazole would also recover. We repeated the experiment and allowed
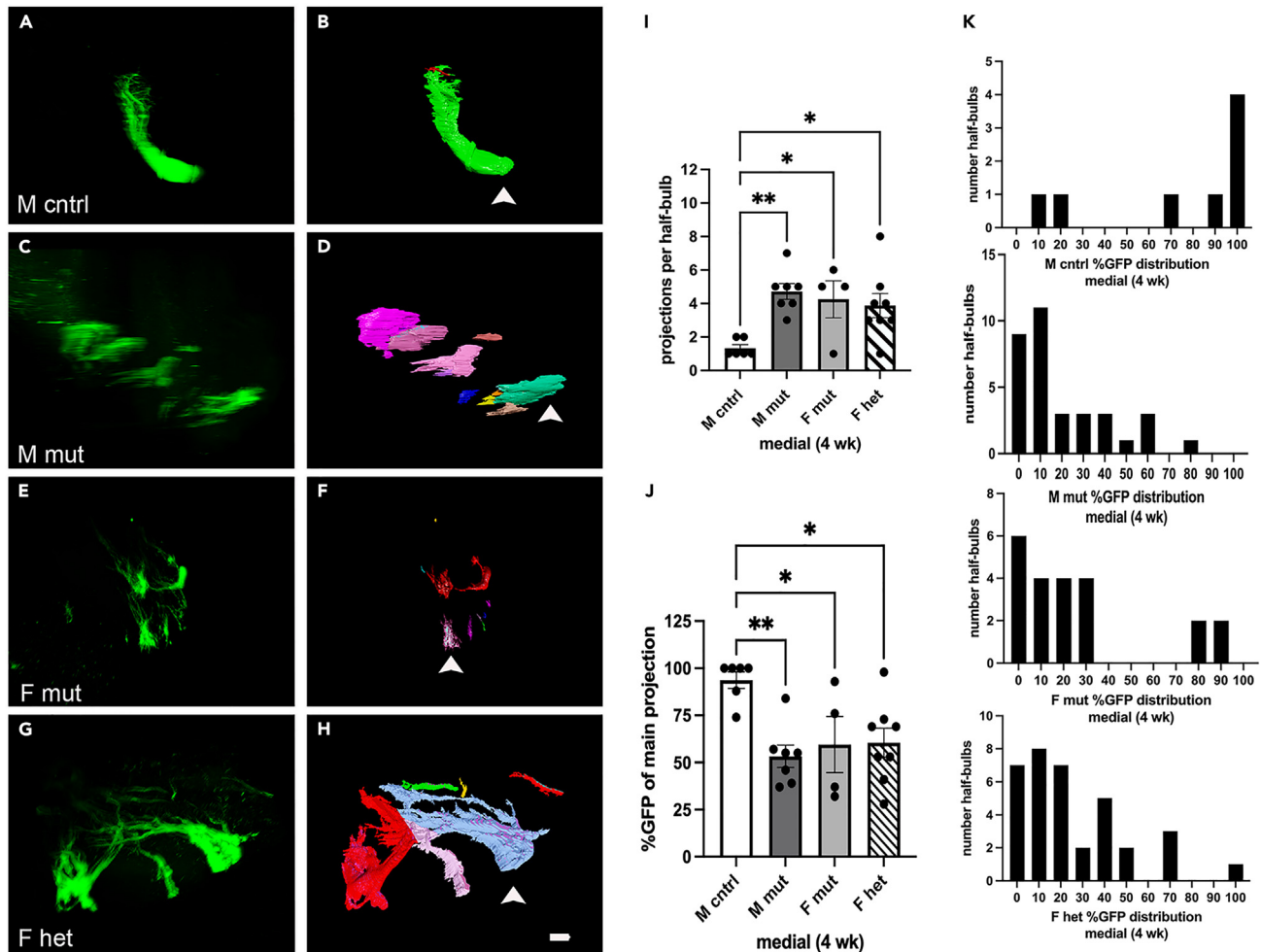
Figure 4. The *Pcdh19^E48X* mutation affects MOR28 OSN medial coalescence during regeneration

(A–H) Projection of image stack obtained by light sheet microscopy (A, C, E, and G) and segmented to define projection patterns on the medial surface (B, D, F, and H). Arrowheads indicate primary glomerular projection based on percent GFP expression relative to other projections.

(I) The number of medial projections per half-bulb is increased in mutant and heterozygous animals; (J) The percent GFP present in the main medial projection is also different relative to control.

(K) Histogram of distribution of GFP expression within each projection (greater than 3%) in the various genotypes. Scale bar: 100 μm. One-way ANOVA (I) $F_{(3,21)}$ = 5.377 (J) $F_{(3,21)}$ = 5.382. Dunnett's test. *$p < 0.05$, **$p < 0.01$. n=6 (M cntrl), 7 (M mut), 4 (F mut), and 8 (F het).

mice to recover for seven weeks instead of four (Figures 5A–5H). At this time point, the number of projections on the lateral surface in mutants was not significantly different from control (Figure 5I). The proportion of GFP present in the main projection, however, still differed between male mutants and male controls (Figures 5B, 5D, and 5J). This is evident in the histogram distribution (Figure 5K), which shows the GFP distribution in male mutants is still skewed toward one end of the scale.

We also assessed medial glomeruli at seven weeks, but no significant differences were observed between mutants and controls (Figure S5).

MOR28-GFP OSNs can be subdivided into two major clusters

We had previously shown that randomly isolated OSNs express 0–7 delta protocadherins.[13] But given the expression pattern of delta protocadherins appears grossly similar between embryonic and adult stages, we asked if OSNs that express the same odorant receptor (e.g., MOR28) also express a common subset of delta family members. We assayed single MOR28 OSNs isolated from three-week-old male and female mice using the NanoString platform. In addition to the delta protocadherins, we included multiple representative examples of other cadherin subfamily members. We also included genes known to be important for OSN guidance during development.

MOR28 OSNs did not express an identifiable, stereotyped pattern of delta protocadherin family members. Despite this, several unexpected features were revealed. Strikingly, cluster analysis showed MOR28 OSNs could be subdivided into two large groups (Figure 6A).
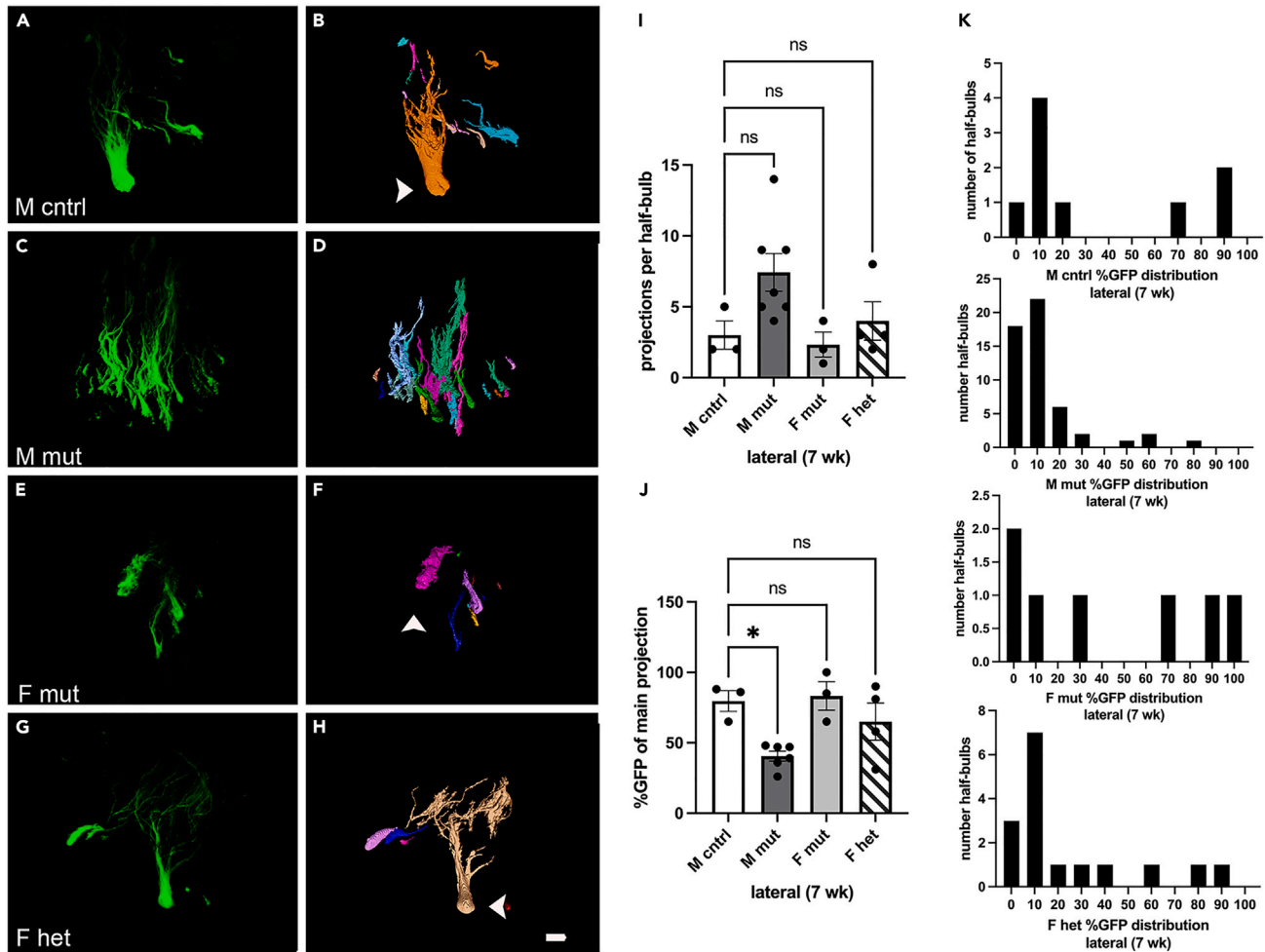
Figure 5. The _Pcdh19^{E48X}_ mutation affects lateral MOR28 coalescence in males at 7 weeks

(A–H) Projection of image stack obtained by light sheet microscopy (A, C, E, and G) and segmented to define projection patterns on the lateral surface (B, D, F, and H). Arrowheads indicate primary glomerular projection based on percent GFP expression.

(I) The number of lateral projections per half-bulb.

(J) The percent GFP present in the main projection is different between male mutants and controls.

(K) Histogram of distribution of GFP expression within each projection (greater than 3%) in the various genotypes. Scale bar: 100 μm. One way ANOVA (J) $F_{(3,12)}$ = 6.012, Dunnett's test. *$p < 0.05$. n = 3 (M cntrl), 6 (M mut), 3 (F mut), and 4 (F het).

[Figure 6](#)B shows an example of a subset of genes with this expression pattern. _Cdh8_, for example, is highly expressed in some OSNs (green dots) and weakly if at all expressed in others (purple dots). _Pcdh17_ displays a similar expression pattern to _Cdh8_. In contrast, _Pcdh19_ is less clearly divided into two groups ([Figure 6](#)B, green cells). Nevertheless, it is apparent that at least a subset of OSNs expresses relatively low levels of _Pcdh19_ (purple cells).

This degree of transcriptional separation was unexpected as all of the assayed OSNs express MOR28, and therefore were predicted _a priori_ to be highly similar to one another. Instead, these clusters indicate a number of cadherin superfamily members and other genes could be used to distinguish MOR28 OSNs. To validate these results, we took two approaches. First, we used single cell qRT-PCR employing a completely different set of primers from that used in the NanoString analysis ([Figure 6](#)C). Genes identified as being differentially expressed among the two clusters (e.g., _Pcdh17_) were confirmed to be expressed in some MOR28 OSNs and not in others, consistent with the existence of the two clusters. _Pcdh8_ is weakly expressed in OSNs based on the NanoString data, and not considered to be statistically differentially expressed among MOR28 OSNs. Our qRT-PCR results confirmed this analysis ([Figure 6](#)C, top row).

One possibility to explain the two clusters is that they indicate OSNs that project to either the medial or lateral glomerulus. Alternatively, OSNs projecting to any one glomerulus may or may not express a given gene, leading to a mosaic pattern of expression within that glomerulus. Some combination of these two possibilities can also be envisioned. We compared the expression pattern of _Pcdh19_ and _Pcdh17_ in MOR28-GFP adults. Using our _Pcdh19_ antibody ([Figures S1](#)I and S1J), fresh frozen cryosections from MOR28-GFP mice were double labeled for _Pcdh19_ and GFP. As indicated ([Figure 6](#)B), _Pcdh19_ expression was detected in MOR28-GFP OSNs in both lateral and medial glomeruli
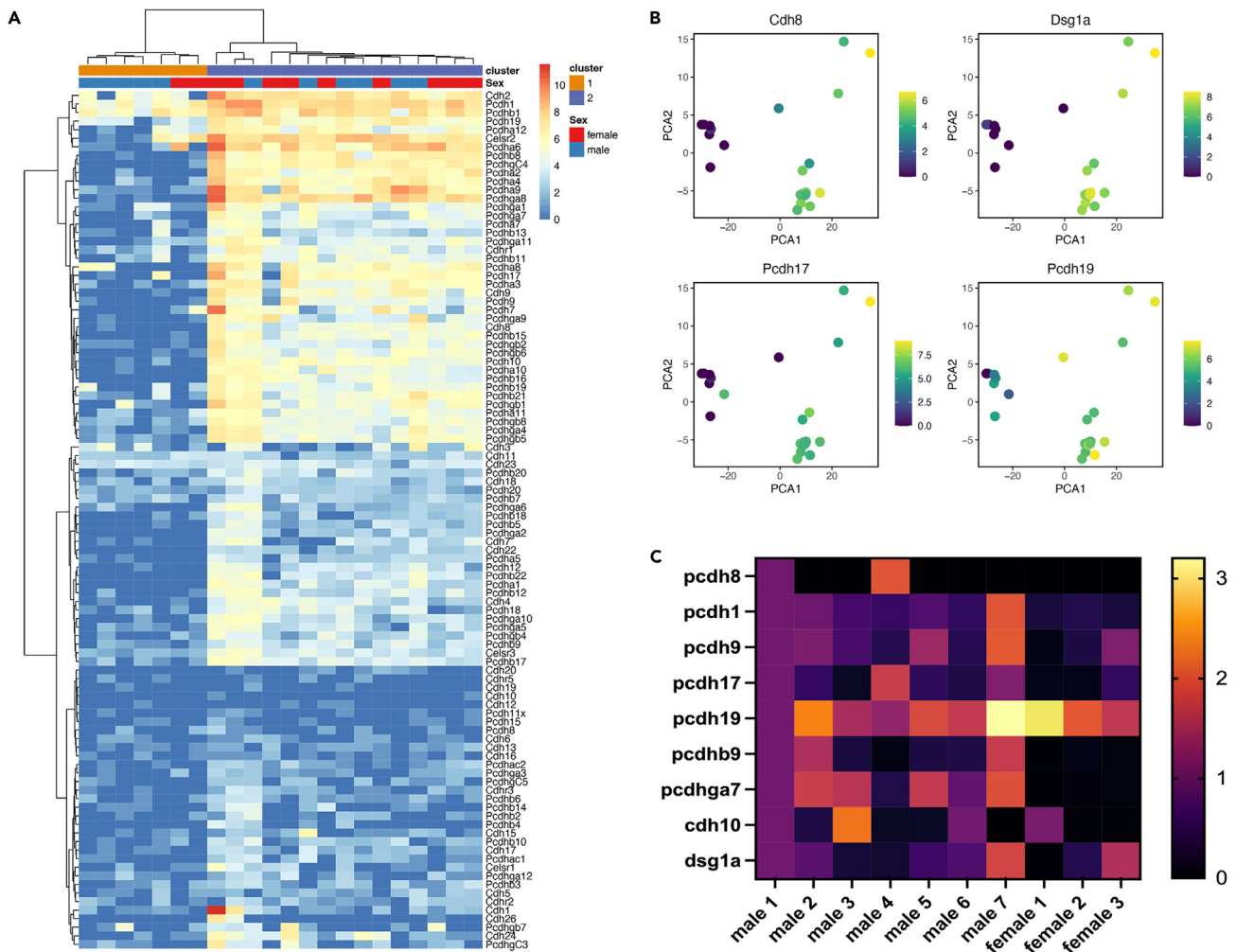
Figure 6. MOR28 OSNs can be subdivided into two large clusters

(A) NanoString analysis followed by clustering of MOR28-GFP positive OSNs shows two clusters.

(B) individual genes (e.g., *Pcdh17*) are expressed relatively highly in some cells (green) or weakly in others (purple).

(C) Single cell qRT-PCR showed variation in expression of identified genes within individual MOR28 OSNs, consistent with the NanoString results.

(Figures 7A–7F). We then examined *Pcdh17* using the same approach. Interestingly, *Pcdh17* was weakly expressed (if at all) in the lateral glomerulus, but more clearly detected in the medial glomerulus (Figures 7G–7L).

NanoString analysis identifies differences in MOR28 OSNs between males and females

Finally, we found males and females can also be distinguished based on the NanoString data. Although the number of individual male and female cells assayed was relatively small, the cluster analysis showed a subset of genes was differentially expressed in females relative to males (Figure 8A). For example, *Pcdh7* is more highly expressed in some female MOR28 OSNs compared to male OSNs (Figure 8B). It is important to note the variation in expression of any given gene within OSNs, as is evident from the heatmap. On average, however, these genes appeared to be more highly expressed in female MOR28 OSNs than in male OSNs.

We confirmed these results using single cell qRT-PCR on male and female OSNs, and again using a completely different primer set from that used in the NanoString analysis. We showed that in general, there was a higher level of expression on average among female OSNs than in males (Figure 8C).

DISCUSSION

Here we show a mutation in *Pcdh19* affects MOR28 OSN coalescence during postnatal stages and regeneration. Unexpectedly, we discovered OSNs that target the lateral aspect of the bulb are more affected. Furthermore, males are more strongly affected than females. The
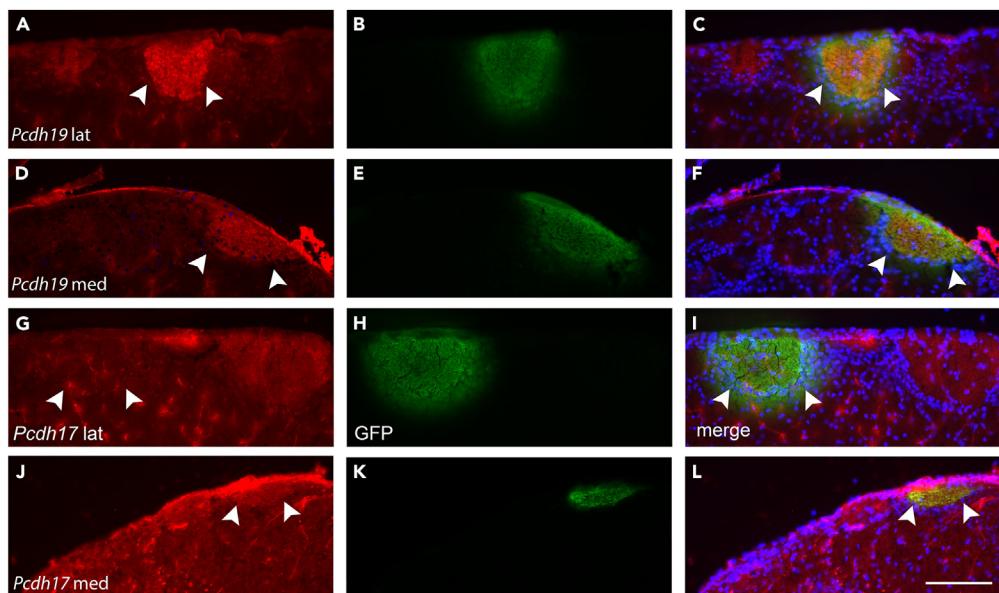
Figure 7. Variation in medial and lateral glomerular expression of delta protocadherins
White arrowheads indicate location of MOR28 GFP⁺ glomeruli.
(A–F) Double labeling to detect PCDH19 (red) and GFP (green) expression shows PCDH19 is present in both lateral and medial MOR28 glomeruli.
(G–I) Double labeling to detect PCDH17 and GFP expression shows minimal detectable PCDH17 in the lateral glomerulus.
(J–L) Weak PCDH17 expression is detected in the medial glomerulus. Scale bar: 100 μm.

presence of numerous cadherin family members and other genes that are differentially expressed among MOR28 OSNs may explain these phenotypes.

The *Pcdh19^E48X* mutant phenotype during postnatal stages is consistent with that seen with other adhesion molecules

Adhesion molecules have long been studied for their potential role in OSN coalescence. These include, for example, classical cadherins, *BIG-2/cntn4*, *Kirrel2/3*, *OCAM* and the clustered protocadherins.[36–42] Other delta protocadherin family members have also been studied. *Pcdh10* expression is regulated by the odorant receptor,[17] and we showed it can affect glomerular position when mis- and over-expressed.[16]

There are significant similarities in phenotype as well as several notable differences between *Pcdh19^E48X* mutants and other adhesion molecules at postnatal stages. Mutations in *BIG-2 (cntn4)* led to an increase in the number of ectopic glomeruli formed by MOR28 OSNs.[38] The number of glomeruli per half bulb seen with *BIG-2* mutants is comparable in scale to that seen with our *Pcdh19^E48X* mutant during development (1.3 vs. ∼1.5 glomeruli/half-bulb in males, respectively). *BIG-2*, however, is not described as being differentially expressed among MOR28 OSNs.

Similarly, deleting *Kirrel2* led to an increase in M72 and MOR174-9 glomeruli. The number of glomeruli increased from two to ∼three glomeruli per whole bulb, on par with the scale of the phenotype observed here during postnatal stages.[41] In contrast to *Pcdh19*, the expression level of *Kirrel 2/3* is relatively uniform within OSNs expressing the same odorant receptor, although there was some mention of variation in expression among OSNs expressing the same receptor.[40] The *BIG-2* and *Kirrel2/3* studies did not describe if medial or lateral glomeruli were differentially affected, or if there were any sex specific effects. Also noteworthy is the fact that *Kirrel3* single,[43] *Kirrel2* single, and *Kirrel2/Kirrel3* double mutants had no impact on MOR28 OSN glomerular number, underscoring the fact that multiple mechanisms and adhesion molecules are involved in glomerular formation.

Mutating the entire Pcdh-alpha subfamily (comprising 14 different family members) led to an increase (∼3- to 5-fold) in the number of lateral glomeruli formed by M71 and MOR23 positive OSNs.[37] A lesser effect (∼2- to 3-fold) was observed for medial glomeruli, paralleling our results showing the lateral glomerulus is more sensitive than the medial glomerulus. No indication was given in this study as to whether or not males or females were differentially affected. In contrast to our data, ectopic glomeruli caused by loss of the alpha Pcdh family persisted throughout the first two months of life. When all clustered protocadherins (comprising ∼60 members in mice) were deleted, protoglomerular formation was severely affected.[39]

Our results therefore bear similarities with other studied genes with unexpected differences as well. In addition to the male/female differences identified here, a notable distinction is the variable degree of expression of *Pcdh19* and other delta family members within MOR28 OSNs. This variable expression of adhesion molecules within MOR28 OSNs adds to the complexity of mechanisms that can influence MOR28 coalescence.
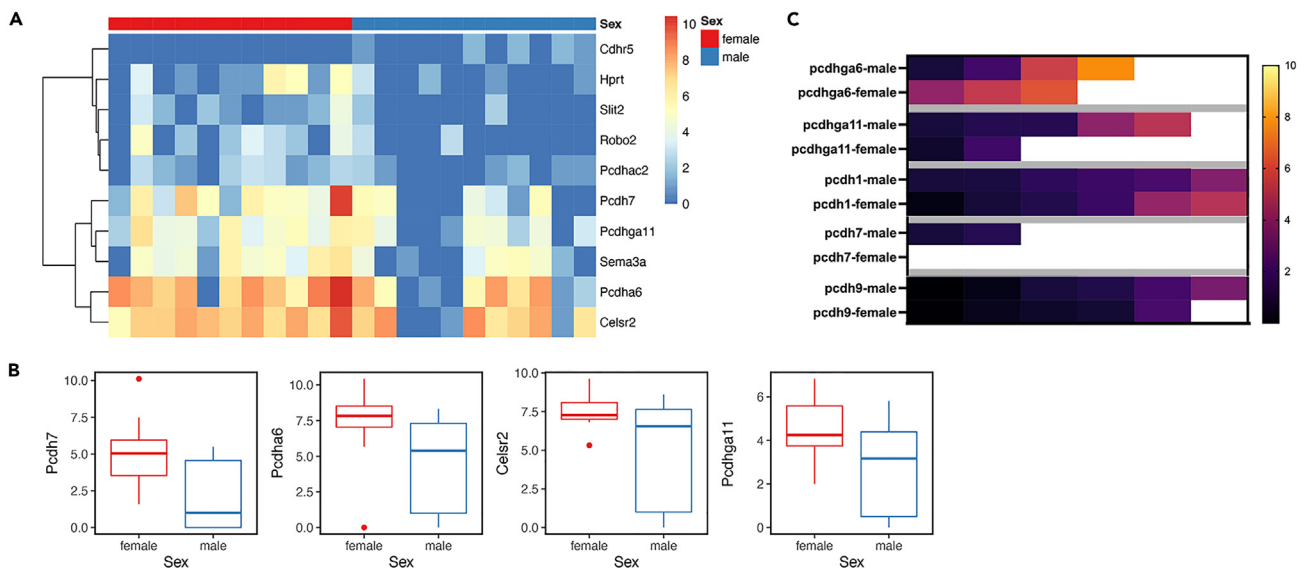
Figure 8. Male and female MOR28 OSNs can be distinguished based on gene expression

(A) Cluster analysis showing the most strongly differentially expressed genes between males and females. Note the variation in expression among different individual OSNs for any given gene.

(B) A subset of the same genes shown in (A) to indicate the difference in median expression between females and males.

(C) Single cell qRT-PCR shows that females tend to have higher expression of some genes. Each box represents a single cell; white boxes indicate higher expression. *Pcdh9* (last two rows) is not predicted by the NanoString data to be statistically different between sexes, consistent with the qRT-PCR data.

It is important to note that mutations in *Pcdh19* are unlikely to affect all OSN populations. Given the large number of guidance cues and cadherin superfamily members expressed by MOR28 OSNs (Figures 6, 7, and 8), the punctate pattern of expression (Figure 1), and our prior results indicating randomly selected OSNs express between 0 and 7 delta family members,[13] OSNs expressing different receptors likely will all display different effects as a result of mutating *Pcdh19*.

Indeed, as has been previously demonstrated,[35,44] different MOR populations display distinct coalescence behavior during development. This is underscored by the fact that different MOR populations coalesce with variable precision to their glomerular positions within the bulb.[45] These differences layer additional complexity on to our understanding of how delta family members may affect OSN regeneration by different populations.

Other mutations in *Pcdh19* have been previously generated which deleted or replaced the first exon.[23,25–27] These mutants showed defects in cortical neuron composition or migration[22,23] but no obvious changes in axon tract formation in the brain. The effects we saw on OSN coalescence may have been possible because of the exquisite resolution afforded by the MOR28-GFP marker. On the other hand, it is also possible that delta family members serve different purposes in different systems.

The *Pcdh19*[E48X] mutation impacts lateral glomeruli more than medial glomeruli

We postulate two possible, non-exclusive explanations why lateral glomeruli are more strongly affected than medial glomeruli. First, the weakly mosaic expression of *Pcdh19* within MOR28 OSNs (Figures 6 and 7) may contribute to this effect. Second, our single cell NanoString data suggests that there are a large number of other cues that regulate medial or lateral coalescence of MOR28 OSNs. While *IGF2* signaling appears to globally influence medial or lateral OSN projection,[46] data from our *Pcdh19*[E48X] mutant, as well as that of other studied adhesion molecules, indicate the presence of further fine-tuning mechanisms within OSNs as they approach their terminal position.

Because two clusters were identified based on our NanoString data, we speculated that some of these genes may be expressed by OSNs that project medially or laterally. And indeed, *Pcdh17* appears to be more highly expressed by OSNs projecting to the medial glomerulus (Figure 7). We emphasize that the expression of *Pcdh17* is relatively low, and it is not clear if *Pcdh17* is missing among lateral OSNs, or simply weakly expressed. The relative paucity of good antibodies capable of specifically detecting delta family members is still an ongoing concern. Better markers may reveal more clearly the pattern of *Pcdh17* expression. Nevertheless, these results suggest there are many other differentially expressed delta and cadherin superfamily members among MOR28 OSNs. These genes may be predominantly medially or laterally expressed, or alternatively, differentially expressed among OSNs that target both the medial and lateral aspect.

Our current and prior[13] single cell results show OSNs can express multiple delta protocadherin family members. To better understand how co-expressed delta protocadherins interact to functionally determine the adhesive profile of a cell, we previously performed an extensive study of delta protocadherin adhesion interactions using *in vitro* cell aggregation assays.[13] This analysis demonstrated that *Pcdh19* was a relatively weak adhesion molecule compared to other members of the family. In contrast, *Pcdh17* was one of the strongest. This difference in adhesive strength may provide

a mechanistic basis for understanding how loss of *Pcdh19* differentially affects the medial and lateral glomeruli. The presence of *Pcdh17* on the medial surface can more readily compensate for our mutation in *Pcdh19*. Its relative absence on the lateral surface, conversely, can render these OSNs more susceptible to mutations in *Pcdh19*. Other guidance cues are also likely to contribute to these phenotypes.

We note that differences in convergence at the medial and lateral surface are not limited to MOR28 OSNs, as an examination of P2 OSNs showed different numbers of glomeruli form at the medial and lateral surfaces.[35] Whether or not other OSN populations can also be subdivided into clusters based on gene expression remains to be determined.

The *Pcdh19^E48X^* mutation appears to affect males more than females during postnatal stages and regeneration

We also found differences in the impact of *Pcdh19^E48X^* mutant on coalescence in males and females. Males were more strongly affected both during postnatal stages and during regeneration (Figures 2, 3, 4, and 5). Our single cell studies suggest a potential rationale for the sex specific differences we observed during MOR28 OSN regeneration. Although the number of individual sex specific cells used for the NanoString analysis is relatively small, we found subtle differences in expression of adhesion molecules between MOR28 OSNs isolated from males and females (Figure 8). We emphasize that these differences are not absolute (e.g., male vs. female) but rather female OSNs appear to be more likely to express these particular genes within MOR28 OSNs. This may explain why females are more resistant to the effects of the mutation because they express additional and/or higher levels of genes that can compensate for mutations in *Pcdh19*. We note that a delta protocadherin family member (*Pcdh20*) has been shown to be differentially expressed in male vs. female glomeruli.[15] Although males showed greater numbers of *Pcdh20* expressing glomeruli than females, this result is consistent with our observed sexually dimorphic gene expression.

Pcdh19 function during postnatal stages and regeneration

Elsewhere in the nervous system, neuronal populations are generally not replaced when lost. Nevertheless, it is useful to compare and contrast lessons learned in other model systems to the olfactory system. Genes expressed during development can be maintained in expression or down regulated in adulthood. Those that are maintained can also be repurposed in adulthood. *Netrin/DCC*, for example, is important for axon guidance during development, but in the adult nervous system regulates synaptic plasticity.[47] When neurons in the CNS or elsewhere in the PNS are injured, transcriptomic studies show this injury can induce a complex network of regeneration associated genes (RAGs).[48–50] These cell-intrinsic features are complemented by cell extrinsic changes, which modulate the permissiveness of the environment for regeneration.

Given the grossly similar expression pattern for *Pcdh19* between embryonic and adult stages (Figure 1), it appears that *Pcdh19* is not induced in response to regeneration. Moreover, during both postnatal stages and methimazole-induced regeneration, *Pcdh19* has an impact on OSN coalescence. Lateral glomeruli appear more affected at both stages, and males were also more affected. Thus, at least this impact of mutating *Pcdh19* appears to be similar at both stages, suggesting this particular function has not been grossly modified during adulthood.

While we have focused on how *Pcdh19* is important for this process, it is clear *Pcdh19* is just one adhesion molecule among many. Moreover, we have not explicitly examined the role of activity in regeneration. Odorant-evoked activity is clearly essential for coalescence during development, and acts to regulate adhesion molecules such as *Kirrel2/3*[40] and *Pcdh10*.[17] Whether or not such activity is also important for regeneration has not yet been studied.

Finally, it is clear from studies of delta *Pcdh17* that the intracellular domain is an important modifier of adhesive interactions.[51] Thus, how intracellular signaling plays a role in regulating *Pcdh19* function is also yet to be determined.

Limitations of the study

We began these studies as a means to test the proposed adhesion model of regeneration. This model was built in part upon the observation that later born OSNs project relatively directly to their glomerular position, suggesting they may be following navigator neuron axons.[10] While we have attempted to test this model by using methimazole to force widespread regeneration, we cannot guarantee complete ablation of the epithelium and fragments of axons may remain. And while we have presumed that loss of the adhesive properties of *Pcdh19* is primarily responsible for these phenotypes, it is conceivable that a signaling component associated with the intracellular domain may be responsible. How *Pcdh19* interacts with other family members or guidance cues *in vivo* is also still unknown.

In conclusion, we have identified *Pcdh19* as a mediator of OSN coalescence during postnatal stages and regeneration. This is the first molecule to be identified in OSN adult regeneration. We uncovered differential effects on medial and lateral glomeruli, and on male and female mutant mice.

STAR★METHODS

Detailed methods are provided in the online version of this paper and include the following:

- KEY RESOURCES TABLE
- RESOURCE AVAILABILITY
  - Lead contact
  - Materials availability

- ○ Data and code availability
- ● EXPERIMENTAL MODEL AND STUDY PARTICIPANT DETAILS
- ● METHOD DETAILS
  - ○ *In situ* hybridization
  - ○ Animal care and handling
  - ○ Generation of *Pcdh19^{E48X}* mice
  - ○ Methimazole ablation
  - ○ Whole mount GFP visualization
  - ○ K562 cell transfection
  - ○ Tissue clearing and light sheet microscopy
  - ○ Light sheet image analysis
  - ○ Antibody staining
  - ○ Single cell isolation and NanoString analysis
  - ○ NanoString analysis
  - ○ Single cell validation
- ● QUANTIFICATION AND STATISTICAL ANALYSIS

SUPPLEMENTAL INFORMATION

Supplemental information can be found online at https://doi.org/10.1016/j.isci.2023.108220.

AUTHOR CONTRIBUTIONS

A.P.M., A.C., S.H., A.J.B., and E.O.W. (investigation, methodology), Y.L. and Y.C. (formal analysis), J.Y.K. (supervision), J.Y.H.Y. (formal analysis and review and editing), D.M.L. (conceptualization, writing, review, and editing).

DECLARATION OF INTERESTS

We, the authors, have a patent related to this work.

INCLUSION AND DIVERSITY

We support inclusive, diverse, and equitable conduct of research.

REFERENCES

1. Dorrego-Rivas, A., and Grubb, M.S. (2022). Developing and maintaining a nose-to-brain map of odorant identity. Open Biol. *12*, 220053. https://doi.org/10.1098/rsob.220053.

2. Yu, C.R., and Wu, Y. (2017). Regeneration and rewiring of rodent olfactory sensory neurons. Exp. Neurol. *287*, 395–408.

3. Mombaerts, P., Wang, F., Dulac, C., Chao, S.K., Nemes, A., Mendelsohn, M., Edmondson, J., and Axel, R. (1996). Visualizing an olfactory sensory map. Cell *87*, 675–686.

4. Ressler, K.J., Sullivan, S.L., and Buck, L.B. (1994). Information coding in the olfactory system: evidence for a stereotyped and highly organized epitope map in the olfactory bulb. Cell *79*, 1245–1255.

5. Vassar, R., Chao, S.K., Sitcheran, R., Nuñez, J.M., Vosshall, L.B., and Axel, R. (1994). Topographic organization of sensory projections to the olfactory bulb. Cell *79*, 981–991.

6. Lodovichi, C. (2021). Topographic organization in the olfactory bulb. Cell Tissue Res. *383*, 457–472. https://doi.org/10.1007/s00441-020-03348-w.

7. Sakano, H. (2020). Developmental regulation of olfactory circuit formation in mice. Dev. Growth Differ. *62*, 199–213. https://doi.org/10.1111/dgd.12657.

8. Ma, L., Wu, Y., Qiu, Q., Scheerer, H., Moran, A., and Yu, C.R. (2014). A developmental switch of axon targeting in the continuously regenerating mouse olfactory system. Science *344*, 194–197.

9. Tsai, L., and Barnea, G. (2014). A critical period defined by axon-targeting mechanisms in the murine olfactory bulb. Science *344*, 197–200.

10. Wu, Y., Ma, L., Duyck, K., Long, C.C., Moran, A., Scheerer, H., Blanck, J., Peak, A., Box, A., Perera, A., and Yu, C.R. (2018). A Population of Navigator Neurons Is Essential for Olfactory Map Formation during the Critical Period. Neuron *100*, 1066–1082.e6.

11. Light, S.E.W., and Jontes, J.D. (2017). δ-Protocadherins: Organizers of neural circuit assembly. Semin. Cell Dev. Biol. 69, 83–90.

12. Pancho, A., Aerts, T., Mitsogiannis, M.D., and Seuntjens, E. (2020). Protocadherins at the Crossroad of Signaling Pathways. Front. Mol. Neurosci. 13, 117. https://doi.org/10.3389/fnmol.2020.00117.

13. Bisogni, A.J., Ghazanfar, S., Williams, E.O., Marsh, H.M., Yang, J.Y., and Lin, D.M. (2018). Tuning of delta-protocadherin adhesion through combinatorial diversity. Elife 7, e41050.

14. Ihara, N., Nakashima, A., Hoshina, N., Ikegaya, Y., and Takeuchi, H. (2016). Differential expression of axon-sorting molecules in mouse olfactory sensory neurons. Eur. J. Neurosci. 44, 1998–2003. https://doi.org/10.1111/ejn.13282.

15. Lee, W., Cheng, T.-W., and Gong, Q. (2008). Olfactory sensory neuron-specific and sexually dimorphic expression of protocadherin 20. J. Comp. Neurol. 507, 1076–1086. https://doi.org/10.1002/cne.21569.

16. Williams, E.O., Sickles, H.M., Dooley, A.L., Palumbos, S., Bisogni, A.J., and Lin, D.M. (2011). Delta Protocadherin 10 is Regulated by Activity in the Mouse Main Olfactory System. Front. Neural Circuits 5, 9.

17. Nakashima, A., Ihara, N., Shigeta, M., Kiyonari, H., Ikegaya, Y., and Takeuchi, H. (2019). Structured spike series specify gene expression patterns for olfactory circuit formation. Science 365, eaaw5030. https://doi.org/10.1126/science.aaw5030.

18. Dibbens, L.M., Tarpey, P.S., Hynes, K., Bayly, M.A., Scheffer, I.E., Smith, R., Bomar, J., Sutton, E., Vandeleur, L., Shoubridge, C., et al. (2008). X-linked protocadherin 19 mutations cause female-limited epilepsy and cognitive impairment. Nat. Genet. 40, 776–781.

19. Kolc, K.L., Sadleir, L.G., Scheffer, I.E., Ivancevic, A., Roberts, R., Pham, D.H., and Gécz, J. (2019). A systematic review and meta-analysis of 271 PCDH19-variant individuals identifies psychiatric comorbidities, and association of seizure onset and disease severity. Mol. Psychiatry 24, 241–251.

20. Depienne, C., and Leguern, E. (2012). PCDH19-related infantile epileptic encephalopathy: an unusual X-linked inheritance disorder. Hum. Mutat. 33, 627–634.

21. Pederick, D.T., Richards, K.L., Piltz, S.G., Kumar, R., Mincheva-Tasheva, S., Mandelstam, S.A., Dale, R.C., Scheffer, I.E., Gécz, J., Petrou, S., et al. (2018). Abnormal Cell Sorting Underlies the Unique X-Linked Inheritance of PCDH19 Epilepsy. Neuron 97, 59–66.e5.

22. Galindo-Riera, N., Newbold, S.A., Sledziowska, M., Llinares-Benadero, C., Griffiths, J., Mire, E., and Martinez-Garay, I. (2021). Cellular and Behavioral Characterization of Pcdh19 Mutant Mice: subtle Molecular Changes, Increased Exploratory Behavior and an Impact of Social Environment. eNeuro 8. ENEURO.0510-20.2021. https://doi.org/10.1523/ENEURO.0510-20.2021.

23. Pancho, A., Mitsogiannis, M.D., Aerts, T., Dalla Vecchia, M., Ebert, L.K., Geenen, L., Noterdaeme, L., Vanlaer, R., Stulens, A., Hulpiau, P., et al. (2022). Modifying PCDH19 levels affects cortical interneuron migration. Front. Neurosci. 16, 887478. https://doi.org/10.3389/fnins.2022.887478.

24. Depienne, C., Bouteiller, D., Keren, B., Cheuret, E., Poirier, K., Trouillard, O., Benyahia, B., Quelin, C., Carpentier, W., Julia, S., et al. (2009). Sporadic infantile epileptic encephalopathy caused by mutations in PCDH19 resembles Dravet syndrome but mainly affects females. PLoS Genet. 5, e1000381.

25. Pederick, D.T., Homan, C.C., Jaehne, E.J., Piltz, S.G., Haines, B.P., Baune, B.T., Jolly, L.A., Hughes, J.N., Gécz, J., and Thomas, P.Q. (2016). Pcdh19 Loss-of-Function Increases Neuronal Migration In Vitro but is Dispensable for Brain Development in Mice. Sci. Rep. 6, 26765.

26. Hayashi, S., Inoue, Y., Hattori, S., Kaneko, M., Shioi, G., Miyakawa, T., and Takeichi, M. (2017). Loss of X-linked Protocadherin-19 differentially affects the behavior of heterozygous female and hemizygous male mice. Sci. Rep. 7, 5801–5815.

27. Hoshina, N., Johnson-Venkatesh, E.M., Hoshina, M., and Umemori, H. (2021). Female-specific synaptic dysfunction and cognitive impairment in a mouse model of PCDH19 disorder. Science 372, eaaz3893. https://doi.org/10.1126/science.aaz3893.

28. Harrison, O.J., Brasch, J., Katsamba, P.S., Ahlsen, G., Noble, A.J., Dan, H., Sampogna, R.V., Potter, C.S., Carragher, B., Honig, B., and Shapiro, L. (2020). Family-wide Structural and Biophysical Analysis of Binding Interactions among Non-clustered δ-Protocadherins. Cell Rep. 30, 2655–2671.e7. https://doi.org/10.1016/j.celrep.2020.02.003.

29. Cooper, S.R., Jontes, J.D., and Sotomayor, M. (2016). Structural determinants of adhesion by Protocadherin-19 and implications for its role in epilepsy. Elife 5, 335.

30. Håglin, S., Bohm, S., and Berghard, A. (2021). Single or Repeated Ablation of Mouse Olfactory Epithelium by Methimazole. Bio. Protoc. 11, e3983. https://doi.org/10.21769/BioProtoc.3983.

31. Blanco-Hernández, E., Valle-Leija, P., Zomosa-Signoret, V., Drucker-Colín, R., and Vidaltamayo, R. (2012). Odor memory stability after reinnervation of the olfactory bulb. PLoS One 7, e46338.

32. Holbrook, E.H., Iwema, C.L., Peluso, C.E., and Schwob, J.E. (2014). The Regeneration of P2 Olfactory Sensory Neurons Is Selectively Impaired Following Methyl Bromide Lesion. Chem. Senses 39, 601–616. https://doi.org/10.1093/chemse/bju033.

33. Tainaka, K., Murakami, T.C., Susaki, E.A., Shimizu, C., Saito, R., Takahashi, K., Hayashi-Takagi, A., Sekiya, H., Arima, Y., Nojima, S., et al. (2018). Chemical Landscape for Tissue Clearing Based on Hydrophilic Reagents. Cell Rep. 24, 2196–2210.e9.

34. Strotmann, J., Conzelmann, S., Beck, A., Feinstein, P., Breer, H., and Mombaerts, P. (2000). Local permutations in the glomerular array of the mouse olfactory bulb. J. Neurosci. 20, 6927–6938. https://doi.org/10.1523/JNEUROSCI.20-18-06927.2000.

35. Royal, S.J., and Key, B. (1999). Development of P2 olfactory glomeruli in P2-internal ribosome entry site-tau-lacZ transgenic mice. J. Neurosci. 19, 9856–9864.

36. Akins, M.R., Benson, D.L., and Greer, C.A. (2007). Cadherin expression in the developing mouse olfactory system. J. Comp. Neurol. 501, 483–497. https://doi.org/10.1002/cne.21270.

37. Hasegawa, S., Hamada, S., Kumode, Y., Esumi, S., Katori, S., Fukuda, E., Uchiyama, Y., Hirabayashi, T., Mombaerts, P., and Yagi, T. (2008). The protocadherin-alpha family is involved in axonal coalescence of olfactory sensory neurons into glomeruli of the olfactory bulb in mouse. Mol. Cell. Neurosci. 38, 66–79.

38. Kaneko-Goto, T., Yoshihara, S.-I., Miyazaki, H., and Yoshihara, Y. (2008). BIG-2 mediates olfactory axon convergence to target glomeruli. Neuron 57, 834–846. https://doi.org/10.1016/j.neuron.2008.01.023.

39. Mountoufaris, G., Chen, W.V., Hirabayashi, Y., O'Keeffe, S., Chevee, M., Nwakeze, C.L., Polleux, F., and Maniatis, T. (2017). Multicluster Pcdh diversity is required for mouse olfactory neural circuit assembly. Science 356, 411–414.

40. Serizawa, S., Miyamichi, K., Takeuchi, H., Yamagishi, Y., Suzuki, M., and Sakano, H. (2006). A neuronal identity code for the odorant receptor-specific and activity-dependent axon sorting. Cell 127, 1057–1069.

41. Vaddadi, N., Iversen, K., Raja, R., Phen, A., Brignall, A., Dumontier, E., and Cloutier, J.-F. (2019). Kirrel2 is differentially required in populations of olfactory sensory neurons for the targeting of axons in the olfactory bulb. Development 146, dev173310.

42. Walz, A., Mombaerts, P., Greer, C.A., and Treloar, H.B. (2006). Disrupted compartmental organization of axons and dendrites within olfactory glomeruli of mice deficient in the olfactory cell adhesion molecule, OCAM. Mol. Cell. Neurosci. 32, 1–14. https://doi.org/10.1016/j.mcn.2006.01.013.

43. Völker, L.A., Maar, B.A., Pulido Guevara, B.A., Bilkei-Gorzo, A., Zimmer, A., Brönneke, H., Dafinger, C., Bertsch, S., Wagener, J.-R., Schweizer, H., et al. (2018). Neph2/Kirrel3 regulates sensory input, motor coordination, and home-cage activity in rodents. Genes Brain Behav. 17, e12516. https://doi.org/10.1111/gbb.12516.

44. Potter, S.M., Zheng, C., Koos, D.S., Feinstein, P., Fraser, S.E., and Mombaerts, P. (2001). Structure and Emergence of Specific Olfactory Glomeruli in the Mouse. J. Neurosci. 21, 9713–9723. https://doi.org/10.1523/JNEUROSCI.21-24-09713.2001.

45. Zapiec, B., and Mombaerts, P. (2015). Multiplex assessment of the positions of odorant receptor-specific glomeruli in the mouse olfactory bulb by serial two-photon tomography. Proc. Natl. Acad. Sci. USA 112, E5873–E5882.

46. Scolnick, J.A., Cui, K., Duggan, C.D., Xuan, S., Yuan, X.-B., Efstratiadis, A., and Ngai, J. (2008). Role of IGF signaling in olfactory sensory map formation and axon guidance. Neuron 57, 847–857. https://doi.org/10.1016/j.neuron.2008.01.027.

47. Horn, K.E., Glasgow, S.D., Gobert, D., Bull, S.-J., Luk, T., Girgis, J., Tremblay, M.-E., McEachern, D., Bouchard, J.-F., Haber, M., et al. (2013). DCC expression by neurons regulates synaptic plasticity in the adult brain. Cell Rep. 3, 173–185. https://doi.org/10.1016/j.celrep.2012.12.005.

48. Chandran, V., Coppola, G., Nawabi, H., Omura, T., Versano, R., Huebner, E.A., Zhang, A., Costigan, M., Yekkirala, A., Barrett, L., et al. (2016). A Systems-Level Analysis of the Peripheral Nerve Intrinsic Axonal Growth Program. Neuron 89, 956–970. https://doi.org/10.1016/j.neuron.2016.01.034.

49. Poplawski, G.H.D., Kawaguchi, R., Van Niekerk, E., Lu, P., Mehta, N., Canete, P., Lie,

R., Dragatsis, I., Meves, J.M., Zheng, B., et al. (2020). Injured adult neurons regress to an embryonic transcriptional growth state. Nature *581*, 77–82. https://doi.org/10.1038/s41586-020-2200-5.

50. Renthal, W., Tochitsky, I., Yang, L., Cheng, Y.-C., Li, E., Kawaguchi, R., Geschwind, D.H., and Woolf, C.J. (2020). Transcriptional Reprogramming of Distinct Peripheral Sensory Neuron Subtypes after Axonal Injury. Neuron *108*, 128–144.e9. https://doi.org/10.1016/j.neuron.2020.07.026.

51. Hayashi, S., Inoue, Y., Kiyonari, H., Abe, T., Misaki, K., Moriguchi, H., Tanaka, Y., and Takeichi, M. (2014). Protocadherin-17 mediates collective axon extension by recruiting actin regulator complexes to interaxonal contacts. Dev. Cell *30*, 673–687.

52. Ritchie, M.E., Phipson, B., Wu, D., Hu, Y., Law, C.W., Shi, W., and Smyth, G.K. (2015). limma powers differential expression analyses for RNA-sequencing and microarray studies. Nucleic Acids Res. *43*, e47. https://doi.org/10.1093/nar/gkv007.

STAR★METHODS

KEY RESOURCES TABLE

REAGENT or RESOURCE	SOURCE	IDENTIFIER
Antibodies		
rat anti-Pcdh19 antibody	BiCell	cat#50539
rat anti-Pcdh17 antibody	BiCell	cat#50537
Rb anti-GFP	Rockland	cat#600-401-215; RRID: AB_828167
Chemicals, peptides, and recombinant proteins		
n-methylnicotinamide	TCM	cat#TCM0374
Antipyrine	VWR	cat#TS10497-1000
butyldiethanolamine	Fisher	cat#154362500
Deposited data		
Nanostring analysis	authors	https://www.maths.usyd.edu.au/u/yingxinl/wwwnb/nanostring/Nanostring_analysis.html https://www.maths.usyd.edu.au/u/yingxinl/wwwnb/nanostring/nanostring_WT_MOR28_counts.csv
Experimental models: Cell lines		
K562 cells	ATCC	cat#CCL-243
Experimental models: Organisms/strains		
Mouse:$Pcdh19^{E48X}$:$Pcdh19^{E48X}$	Lin lab	Lin Lab - $Pcdh19^{E48X}$
Oligonucleotides		
$Pcdh19$-ATG	IDT	atggagtctctcctgctgccgg
$Pcdh19$-CRISPR-rev592	IDT	ccaggctcttctccaccaccagt
Software and algorithms		
limma trend	Ritchie et al., NAR 2015 Apr 20; 43(7):e47.	PMID: 25605792

RESOURCE AVAILABILITY

Lead contact

Further information and request for resources and reagents should be directed to and will be fulfilled by the lead contact, David Lin (DML45@cornell.edu).

Materials availability

The $Pcdh19^{E48X}$ mouse model will be freely distributed to investigators at academic institutions wanting mice for non-commercial research. Use of the mice may require a Material Transfer Agreement, as negotiated by the Cornell Technology Transfer Office. Mice will be provided at no cost, except for shipping associated expenses. If mice are particularly valuable to the community, they will be deposited at the Jackson Laboratory. For for-profit institutions and corporations, use of the mice will be negotiated by the Cornell Technology Transfer Office, and all licensing will be pursuant to Cornell's policy on royalty income, if applicable.

Data and code availability

- The NanoString data reported in this study cannot be deposited in a public repository because it is not considered a standardized datatype. However, the dataset and analysis can be accessed here: https://www.maths.usyd.edu.au/u/yingxinl/wwwnb/nanostring/Nanostring_analysis.html, https://www.maths.usyd.edu.au/u/yingxinl/wwwnb/nanostring/nanostring_WT_MOR28_counts.csv.
- No original code was developed for the analysis.
- Any additional information required to reanalyze the data reported in this paper is available from the lead contact upon request.

EXPERIMENTAL MODEL AND STUDY PARTICIPANT DETAILS

In vivo animal studies –The $Pcdh19^{E48X}$ mice were originally generated in an FVB/B6 background but subsequently outcrossed to FVB mice for six generations prior to being interbred. The MOR28 marker strain is of a mixed 129:B6 background. Mutant mice were bred to the marker strain and the F1 offspring interbred to generate littermates used for this experiment. Mice were maintained at Cornell University under group housing conditions in filter top cages under 13:11 light dark conditions and fed chow *ad libitum*. Male and female mice were used for all experiments. Ages were as described in the text. For the developmental analysis, male and female mice were obtained at P13, P20-22, and six weeks of age. For the regeneration experiments, mice were collected at four and seven weeks post treatment. For the NanoString experiment, mice were approximately 4 weeks of age. As described in the text, we identified significant differences on the impact of sex on the outcomes of this study, as males displayed more severe phenotypes than females. K562 cells were purchased from ATCC (CCL-243).

METHOD DETAILS

In situ hybridization

Fresh frozen epithelia from embryonic day 17 (E17) or adult mice were embedded in OCT (Tissue-Tek) and 20 micron thick sections were collected onto Superfrost Plus slides (VWR) using a Leica CM1950 cryostat. Slides were postfixed in 4% paraformaldehyde buffered with sodium phosphate prior to washing in 0.2X SSC. Slides were then acetylated and blocked in hybridization buffer (50% formamide, 5X SSC, 5X Denhardt's solution, 250 μg/ml tRNA and yeast RNA, 0.1% Tween 20 and 5 mM phosphate buffer pH 7.5) prior to addition of a digoxigenin labeled probe. After hybridization at 60–70°C, slides were washed and incubated with an alkaline phosphatase conjugated anti-digoxigenin antibody (Roche), and then reacted with NBT/BCIP substrates (Promega) as per manufacturer instructions.

Animal care and handling

All animal protocols were reviewed and approved by Cornell's Institutional Animal Care and Use Committee. MOR28-GFP mice were a generous gift of Gilad Barnea and are maintained in a mixed B6:129 background. Female mutants were crossed with MOR28-GFP males to generate hemizygous males and heterozygous females, and F1 animals were intercrossed. Because *Pcdh19* is on the X chromosome, only male control (non-mutant) animals were obtained for comparison. Animals were maintained on a standard chow diet and fed *ad libitum*.

Generation of $Pcdh19^{E48X}$ mice

A guide RNA was generated by creating a template composed of primers surrounding the PAM site. mRNA was generated and sent to the Cornell Transgenic Core for injection into F1 B6/FVB mice. Founders were outcrossed to FVB mice for six generations prior to these experiments to reduce the likelihood of off target effects. Mice are genotyped using primers that amplify the region surrounding the introduced nonsense mutation, and then tested for the presence of the mutation by digesting the PCR product with HindIII. Homozygous and hemizygous mutant mice will only generate the cleaved product, whereas heterozygous mice will have both cleaved and uncleaved PCR bands.

Methimazole ablation

Two to three month-old littermates were weighed and injected intraperitoneally with methimazole (100 mg/kg). We found, as previously described in other studies,[30] more consistent ablation of more ventral OSNs with a higher dose of methimazole. Mice were allowed to recover for four or seven weeks prior to sacrifice.

Whole mount GFP visualization

Whole mount olfactory bulbs still attached to the remainder of the brain were dissected from freshly euthanized animals and visualized with a Leica MZFLIII microscope fitted with a GFP dichroic filter. Images were captured with an Olympus DP70 camera.

K562 cell transfection

K562 cells were maintained in RPMI plus L-glutamine media supplemented with 10% calf bovine serum. One million cells were resuspended in 100 μL of Ingenio Electroporation solution and mixed with five to eight μg of DNA, followed by nucleofection with an Amaxa II nucleofector as per manufacturer's recommendation. Following a 1 h recovery, cells were gently agitated for 1–3 days at 15 RPM prior to imaging, as described.[13]

Tissue clearing and light sheet microscopy

The protocol for tissue clearing is based on Tainaka et al.[33] with the following modifications. Mice were anesthetized with avertin and then transcardially perfused with 20 mls of chilled phosphate buffered saline (PBS) followed by eight mls of phosphate buffered 4% paraformaldehyde (PFA) and 10 mls of PBS. Brains with attached olfactory bulbs were dissected out and fixed overnight with 4% PFA. After several washes with PBS to remove fixative, brains and bulbs were placed in 50% CUBIC-L at 37°C overnight. Samples were changed to 100% CUBIC-L after 24 h and left at 37° for an additional four days. CUBIC-L solution was changed at days one and three during the four day incubation. After washing with PBS, samples were placed in 50% CUBIC-RA for 24 h at room temperature, and then 100% CUBIC-RA for at least 24 h prior to embedding. Brains were bisected laterally and half was embedded in CUBIC-RA containing 1.6% agarose in PMMA cuvettes.

Samples were imaged with the LaVision Bio Tec Light sheet Ultramicroscope II. Bulbar structure was illuminated using the 640 nm laser, and GFP signal visualized at 480 nm. All images were taken at the same magnification with a z axis step size of 10 μm. Because samples had one or two GFP markers present, laser power for each channel was adjusted accordingly for each sample to maximize intensity distribution.

Light sheet image analysis

Images were uploaded to Arivis 4D 3.5. Using the GFP signal detected by the 488-laser, an intensity threshold was set as determined by the intensity of the GFP signal to be able to segment the projections. Thresholds ranged from 5000 to 7000 for each medial and lateral sample, given that some mice possessed two copies of the MOR28 transgene and others one. Segmentation was confirmed in 2D prior to object identification in 3D. Once projections were segmented, the sum-intensity of each projection was calculated based on GFP signal intensity. Objects that were inaccurately segmented together were split using an automated filter set at 50% sensitivity.

Antibody staining

Twenty micron thick fresh frozen sections were collected onto Superfrost Plus (VWR) slides and postfixed in freshly made 4% phosphate buffered paraformaldehyde. Samples were washed and permeabilized in PBS containing 0.2% Tween 20 and blocked in the same solution containing 10% heat inactivated fetal bovine serum. Antibodies in block were applied overnight at 4°, washed, and then reacted with an Alexa Fluor 547 conjugated secondary (Jackson Immunoresearch). Sections were mounted in 70% glycerol containing DAPI and anti-fade and imaged on a Leica DMRE upright microscope fitted with an Andor Xyla camera. Primary antibodies (PCDH19 (cat#50539) and PCDH17 (cat#50537)) were purchased from BiCell.

Single cell isolation and NanoString analysis

After visually separating the two sexes, epithelia from males or females were dissected out in 1x Modified Eagles Medium with Temin's modification. Epithelia were dissociated with the Papain Dissociation System (Worthington Biochemical) followed by fluorescence-activated cell sorting to isolate individual GFP positive OSNs. Single cells were hybridized and assayed with the NanoString platform, as described previously.[13]

NanoString analysis

A set of ~200 genes were chosen to assay. We first performed $\log_2$ transformation of the raw count data, and then performed hierarchical clustering on the dataset with Euclidean distance and ward.D2 as the clustering method to cluster cells into two clusters. We then visualized the data using principal components analysis, where the first two principal components are visualized. Finally, we performed limma-trend[52] to select the genes that are differentially expressed between the sexes.

Single cell validation

Single MOR28 OSNs from male and female mice were isolated by fluorescently activated cell sorting. Cells were collected into lysis buffer and amplified using the CellsDirect One step qRT-PCR kit from Invitrogen.[13] Primers used for the qRT-PCR are described in Table S1.

QUANTIFICATION AND STATISTICAL ANALYSIS

Prism (9.0) was used for all statistical analyses. The specific statistical tests used are described in the figure legends.